LU-TP 21-27
June 2021

Event Geometry and Anisotropic Flow in Proton-Proton Collisions

Johannes Holst

Department of Astronomy and Theoretical Physics, Lund University

Bachelor thesis supervised by Christian Bierlich

LUND
UNIVERSITY

Abstract

We seek to better understand the relationship between an anisotropic distribution of partons in the initial state of pp-collisions and the amount of elliptic flow. We do this through the implementation of a new model that is based in generating positions for multiparton interactions from the uneven volume created by the overlap of two Gaussians. We then examine how this asymmetric probability density function compares to geometries without intrinsic anisotropy and data from the CMS and ALICE. This is achieved by simulations based in these geometries in a hydrodynamical toy model and in PYTHIA.

Popular Science Abstract

At the Large Hadron Collider (LHC) in Switzerland protons are being collided at velocities near the speed of light. This is done to study how matter behaves under very hot and dense conditions. Despite the continuous improvement and success of previous models we still lack an exact theory for how the particles that make up protons behave at these high temperatures and densities.

One key observation from research at the LHC has been what is known as anisotropic flow. It is a liquid-like motion of the particles flying out of the colliding protons. The reason they behave this way is believed to be because of the collision geometry being lopsided. This means that when the protons collide, they rarely do so head on and the collision region is therefore more closely packed in some directions than others. When the system then expands the particles are sprayed more in some directions than others.

Conventionally, flow would be described in terms of Quark-Gluon Plasma (QGP), a state of matter where the particles are deconfined from the proton structure. It is believed to be what constituted the very first microseconds of the universe. QGP explanations of flow are generally combined with hydrodynamical models and widely applied in fairly accurate computer simulations of these events. Although, it is still an open question whether observations of flow necessarily presuppose QGP.

The PYTHIA event generator simulates the collective mechanisms associated with flow using the Lund String Model (LSM). The LSM models these flow effects by string shoving, which means describing the particles as being tied up into strings that then interact with each other by pushing, forming ropes and fragmenting into other particles. The reason it is of value to us is because it is not reliant on QGP and hydrodynamics, so if these models are more consistent with experiments it may cause us to reevaluate our theories.

In this project a set of different geometries for describing the spatial distributions of particles in the interaction region will be implemented in both hydrodynamical QGP and PYTHIA models. The different geometries rely on a variety of mathematical and empirical descriptions for how interactions are to be distributed in the initial state of the collision. Then computer simulations of anisotropic flow are run based on these probability functions. Finally, the results of each model will be compared to experimental data from the LHC. The purpose of the project is to examine and evaluate the different models and observations. In order to keep improving our understanding of how the world works and how it came to be, we need further research in the comparison between the predictions of our descriptions and the empirical observations.

Contents

List of acronyms

LHC : Large Hadron Collider
QCD : Quantum Chromodynamics
LSM : Lund String Model
ALICE : A Large Ion Collider Experiment
RHIC : Relativistic Heavy Ion Collider
QGP : Quark-Gluon Plasma
CMS : Compact Muon Solenoid
MPI : Multiparton Interaction

List of Figures

1 Introduction

Protons are *hadrons* made up of *partons*. These partons are called quarks and gluons. The gluons are the carriers of the *strong force* which binds the quarks into hadrons. At the Large Hadron Collider (LHC) and the Relativistic Heavy Ion Collider (RHIC) hadrons and heavy ions are being collided at high velocities in order to study how hadronic matter behaves under extreme energy densities. When the heavy ions or protons collide one can observe *elliptic flow*, an azimuthal asymmetry in the final state of the collision [1]. This can be understood as a response to the anisotropy in the initial state geometry. What this means is that the active area for parton collisions becomes lopsided by the impact parameter, and as such more hadrons are observed at some angles in the event plane than others [2]. This relationship between the eccentricity in the initial state geometry and the amount of elliptic flow has been observed and described at the RHIC [3]. Figure 1 shows a cartoon of the distribution of charges and parton interactions in a collision event where the two circles are protons and b is their impact parameter.

The high density of the colliding proton constituents is predicted to deconfine them to form a rapidly expanding hot and dense collection of free-moving quarks and gluons. This state of matter is conventionally described in terms of a thermalized medium called *Quark-Gluon Plasma* (QGP). Models based in hydrodynamical descriptions of QGP have also been quite successful in simulating flow in agreement with the data. Though this does not necessitate the existance of QGP [4].

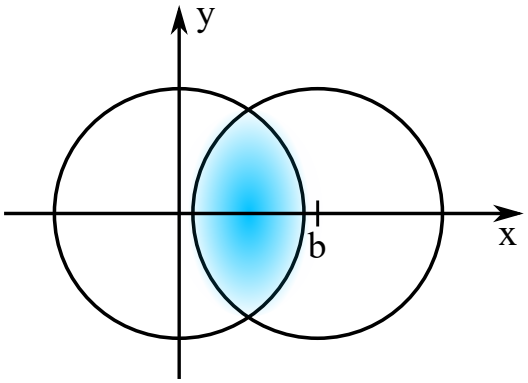

Figure 1: Cartoon of a pp-collision viewed in the direction of the beam.

One model which is not reliant on QGP is the *Lund String Model* (LSM), which is applied in an event generator called PYTHIA, where the collective mechanisms are modelled through treating the color field between interacting quarks as strings [5]. The color field is the confining force between color charges and can be thought of as the strong force equivalent to the electromagnetic field between opposite electric charges. Unlike the electric field the color field forms a narrow flux tube, which is what the strings represent. The color flux tubes between confined partons repel at high densities due to the compression of the color field, analogues to the repulsion caused by the opposite flux of the magnetic fields of two dipoles. It can thereby explain a similar anisotropic expansion of the interaction region to that of the hydrodynamical QGP treatment.

The purpose of the project is to simulate the anisotropy in the final state momentum distribution through generating initial positions of parton interaction vertices from an

asymmetric probability density function. We do this in order to gain insight into how the elliptical shape of quarks and gluons spatial arrangement impacts elliptic flow. We will attempt this by introducing a new model which describes two colliding protons in the transverse plane as two-dimensional Gaussians and uses their asymmetric overlap region to generate parton positions in the initial state of the collision. Then we use this initial spatial distribution of parton interactions to simulate the final state momenta distribution and thereby the amount of elliptic flow. We will do this in both a hydrodynamical toy model based on an empirical formula from the RHIC and through the LSM in PYTHIA. In both cases we will be evaluating how this model performs in relation to other models by direct comparison to the measurements of elliptic flow in proton-proton collisions from the Compact Muon Solenoid (CMS) detector and A Large Ion Collider Experiment (ALICE) at the LHC.

The thesis is structured starting with section 2, which outlines the foundation for the theory relating to the geometry of proton collisions, anisotropic flow and the PYTHIA MPI model. In section 3 the method is presented. This includes the analytic derivation of the overlap model, the creation of the toy model and the implementation into PYTHIA. In section 4 the results are presented and section 5 features the discussion and conclusions.

2 Theory

2.1 Multiparton Interactions

Protons consist of two up quarks and one down quark bound by gluons. Early ideas of modelling collisions of protons would describe the phenomenology in terms of single parton-parton interactions, but these could not account for the high activity observed in experiments. Which is why we will be modelling in terms of *multiparton interactions* (MPIs), where each proton-proton collision contains several parton-parton collisions [6]. The PYTHIA MPI model consists of a single unified framework for describing multiparton interactions with both soft QCD processes like scattering and fragmentation and hard QCD processes such as parton showers and hadronization. By integrating the regulated parton-parton cross section one finds a rough estimate of the number of MPIs in each average inelastic non-diffractive hadron-hadron collision as

$$\langle N_{MPI} \rangle (p_{\perp 0}) = \frac{\sigma_{2\to 2}(p_{\perp 0})}{\sigma_{ND}}, \tag{2.1}$$

where $\langle N_{MPI} \rangle (p_{\perp 0})$ is the average number of MPIs, $\sigma_{2\to 2}(p_{\perp 0})$ is the regulated parton-parton cross-section integrated with respect to transverse momentum, σ_{ND} is the non-diffractive cross-section and $p_{\perp 0}$ is a parameter meant to tame the divergence of the cross section for low transverse momenta. This is done since the physical cross-section is inversely proportional to transverse momenta and as such diverges for low values. Adding the free

parameter $p_{\perp 0}$ to the denominator therefore tames this divergence. This formula treats the MPIs as independent and equivalent but in PYTHIA the distribution of the number of MPIs is narrower due to correlative effects such as conservation of parton momentum being taken into account [7].

2.2 Geometry of Proton Collisions

The formalism that will be adhered to is the description of the relativistic protons as probability density distributions of partons in transverse space. More specifically as normalized intersecting Gaussians whose means are separated by their impact parameter. It may seem intuitive to model the protons as uniform density spheres, which is one of the alternatives available in PYTHIA. The problem with this is twofold: the charge distribution of protons is not uniform and secondly one can not generate events where the impact parameter is greater than the diameter of the proton.

Describing the charge distributions of the protons as Gaussians is fairly straightforward, since in electron scattering experiments the proton radius is measured in terms of what is called the root-mean-square radius of the charge distribution [8]. If this is used as the mean of a normalized three-dimensional Gaussian the result is a probability density function which is an accurate approximation of a proton from which parton positions can be generated. At high velocities the significant Lorentz length contraction allows for the description of protons as two-dimensional Gaussians. The radius of the protons is also dependent on the energy of the collision [9]. At 13 TeV the default standard deviation of the proton Gaussian in PYTHIA is around 0.7 fm. We define the Gaussians for each proton as

$$G_1(x, y) \equiv \frac{1}{2\pi\sigma^2} \exp\left(-\frac{x^2 + y^2}{2\sigma^2}\right) \tag{2.2}$$

$$G_2(x, y) \equiv \frac{1}{2\pi\sigma^2} \exp\left(-\frac{(x - b)^2 + y^2}{2\sigma^2}\right). \tag{2.3}$$

Where b is the impact parameter separating the means of the Gaussians and σ is their standard deviation.

The default way of generating positions for the parton vertices in PYTHIA makes use of the convolution of two Gaussians [7]. This corresponds to the addition of the random variables in each Gaussian and results in another normalised Gaussian from which MPI vertices are calculated. Though the convolution model more accurately represents how there are higher probability densities towards the center of the distribution than the above mentioned sphere model, it lacks any intrinsic spatial anisotropy.

In heavy ion collisions the final state anisotropy can be modelled by means of nucleon sources travelling along straight lines and asymmetrically spraying nucleons after being

"wounded" by the collision [10]. As an extension one can model the anisotropy in pp-collisions with wounded quarks emitting independent particles [11]. But this means of modelling "wounded" sources travelling along straight lines does not translate well into PYTHIA. This is because PYTHIA describes a rapidity distribution which does not neatly separate transverse and longitudinal particles like the wounded quark models do.

2.3 Anisotropic Flow

As can be seen in figure 1 the distribution in the collision forms an almond shape. The anisotropy in this distribution will cause more partons to be ejected in the direction of the impact parameter than perpendicular to it. This anisotropy in final-state momentum as caused by the elliptic distribution of the collision geometry is quantifiable through the flow harmonics, which are the coefficients of the Fourier expansion for the particles momentum-space distribution. [5]

$$E\frac{d^3N}{d^3p} = \frac{1}{2\pi}\frac{d^2N}{p_\perp dp_\perp dy}\left(1 + 2\sum_{n=1}^{\infty} v_n \cos(n(\Phi - \Psi_n))\right) \tag{2.4}$$

Where Φ is the azimuth and Ψ_n is the reaction plane. The reason that there is no sine term is because of the symmetry of the reaction plane. We will focus on $v_2\{2\}$, the elliptic flow harmonic calculated from two-particle correlation.

One means of modelling the anisotropic flow is through QGP which expand in accordance with ideal hydrodynamics. An empirical formula from RHIC [12] which has been successful is

$$v_2\{2\} = \epsilon\{2\}\left(\frac{v_2}{\epsilon}\right)_{hydro}\frac{1}{1 + \frac{\lambda}{K_0}\frac{\langle S\rangle}{\langle\frac{dN}{d\eta}\rangle}}. \tag{2.5}$$

Where $\epsilon\{2\}$ is the eccentricity of the collision geometry, $\left(\frac{v_2}{\epsilon}\right)_{hydro} \approx 0.2$ is the ideal hydrodynamics result and $\frac{\lambda}{K_0} = 5.8\ \text{fm}^{-2}$ is the amount of incomplete equilibration. $\langle S\rangle$ is the area and $\langle\frac{dN}{d\eta}\rangle$ is the distribution of total hadron rapidity. The triangular brackets denote the average over events.

From this equation and figure 1 we can make a few observations about how these quantities relate to the impact parameter of the collision. The greater the impact parameter the smaller and narrower the area gets and thus the number of particles in the overlap of the distributions shrinks while the eccentricity increases. Or more simply, at a fixed number of particles the amount of elliptic flow is directly proportional to the eccentricity of the parton distribution.

The ideal liquid-like expansion of the thermalized medium relates the initial state eccentricity and the final asymmetry in the azimuth from the pressure gradients in each direction. The pressure in the center of the almond is uniform and the pressure outside the almond

is zero. Therefore the pressure gradient must be greater in the x direction and more final state hadrons are sent out along that axis when the interaction region expands.

2.4 String Shoving

In the LSM the color field flux tubes between quarks is described by a massless string that connects the outgoing partons with a string tension $\kappa = 1$ GeV/fm. During the system expansion the outgoing partons transfer kinetic energy to the string. At sufficient energies it will eventually be favourable for the string to break. The final state hadrons are then identifiable as the fragmented string pieces.

For most color charge dipole combinations the flux has opposite orientation. The color fields on parallel strings overlap and the opposite orientation of the flux causes the color field to be compressed and the strings to expand transversely. This repulsion is called *string shoving* and it makes it possible to simulate collective mechanisms in the transverse plane, such as elliptic flow, without hydrodynamics and QGP [13].

The force between the flux tubes is governed by the following equation.

$$f(d_\perp) = \frac{g\kappa d_\perp}{R^2} \exp\left(-\frac{d_\perp^2(t)}{4R^2}\right) \tag{2.6}$$

Where R is the width of the Gaussian for the flux tubes' time dependent energy distribution, $d_\perp$ is the transverse separation between flux tubes, κ is the string tension and g is a tunable parameter that is equal to one if a longitudinal color-electric field is dominating the energy in the flux tube. Because of the explicit dependence of the transverse separation between the tubes this way of modelling collective mechanisms also encapsulates the effects of the initial state eccentricity on the flow harmonics.

Unlike the hydrodynamical formula (2.5) that directly correlates initial state positional anisotropy with final state azymuthal asymmetry, the string shoving model has time dependence both in R and $d_\perp$ which grants a more microscopic picture of the evolution of the collision.

3 Method

3.1 Probability Density Functions

Here three different probabilistic geometries for generating parton positional data in the initial state of the collision will be derived and studied analytically. The first geometry is the convolution model which uses the convolution of the two Gaussians as its probability density function. It is the default distribution for simulating the collision geometry

in PYTHIA and corresponds to the addition of the random variables for both proton Gaussians. We can represent this as

$$(G_1 * G_2)(x, y) = \int_{-\infty}^{\infty} G_1(\tau) G_2(x - \tau) d\tau \cdot \int_{-\infty}^{\infty} G_1(\upsilon) G_2(y - \upsilon) d\upsilon.$$

Which works out to be

$$(G_1 * G_2)(x, y) = \frac{1}{4\pi\sigma^2} \exp\left(-\frac{(x-b)^2 + y^2}{4\sigma^2}.\right) \tag{3.7}$$

Secondly we have the product model which is the geometry described by multiplying the Gaussians with each other. Instead of sampling a collective distribution for both Gaussians like the convolution model does, the product model treats the random variables as independent choices. We write this as

$$(G_1 \cdot G_2)(x, y) = \frac{1}{4\pi^2\sigma^4} \exp\left(-\frac{(x-b)^2 + x^2 + 2y^2}{2\sigma^2}\right)$$

The inverse of the integral of the product of the Gaussians will give the normalization constant

$$K_\times = \left(\int_{-\infty}^{\infty}\int_{-\infty}^{\infty} (G_1 \cdot G_2)(x, y) dy dx\right)^{-1} = 4\pi\sigma^2 \exp\left(\frac{b^2}{4\sigma^2}\right)$$

So the normalized product is

$$K_\times (G_1 \cdot G_2)(x, y) = \frac{1}{\pi\sigma^2} \exp\left(-\frac{(x - b/2)^2 + y^2}{\sigma^2}\right). \tag{3.8}$$

The third geometry is the overlap model which describes the probability distribution as the region of overlap between the two Gaussians.

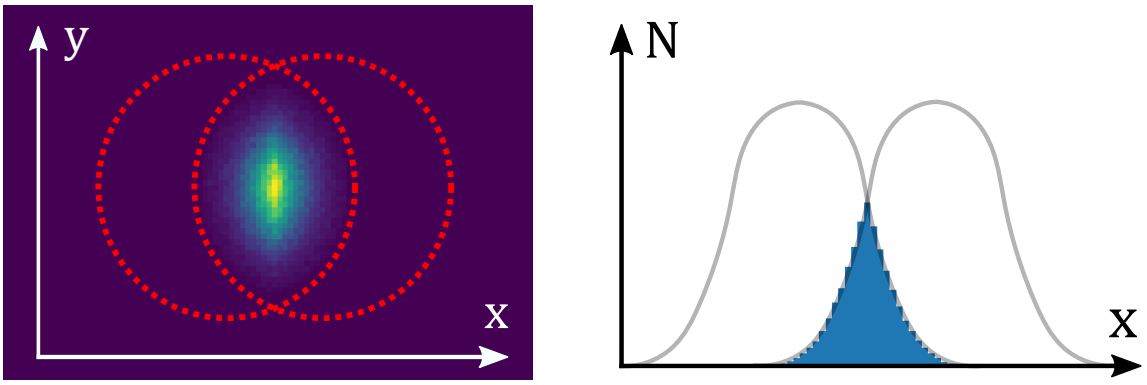

Figure 2: Two sketched histograms illustrating the overlap model. On the left is a histogram in the xy-plane and on the right we have the same histogram with number of events, N, on the y-axis.

This model encapsulates something important that the other two geometries do not, namely the positional anisotropy in the initial state. More specifically it describes how the eccentricity and size of the collision area depends on the impact parameter.

For any two Gaussians this can be very hard to normalize analytically. But if we do not take radial fluctuations into account we can assume that both Gaussians have the same standard deviation and only differ in where their means are on the x-axis

$$G_1(x,y) = G_2(x,y) \iff \frac{1}{2\pi\sigma^2}\exp\left(-\frac{x^2+y^2}{2\sigma^2}\right) = \frac{1}{2\pi\sigma^2}\exp\left(-\frac{(x-b)^2+y^2}{2\sigma^2}\right).$$

Cancelling terms on both sides gives

$$x^2 = (x-b)^2 \iff x = \frac{b}{2}$$

So the plane of intersection between the Gaussians is when $x = \frac{b}{2}$. We can use this to normalize the distribution. The integral over the whole overlap region is

$$\int_{-\infty}^{\infty}\int_{-\infty}^{\infty}(G_1 \cap G_2)(x,y)dydx = \int_{-\infty}^{b/2}\int_{-\infty}^{\infty}G_2(x,y)dydx + \int_{b/2}^{\infty}\int_{-\infty}^{\infty}G_1(x,y)dydx.$$

Integrating with respect to y gives

$$\int_{-\infty}^{b/2}\frac{1}{\sqrt{2\pi}\sigma}\exp\left(-\frac{(x-b)^2}{2\sigma^2}\right)dx + \int_{b/2}^{\infty}\frac{1}{\sqrt{2\pi}\sigma}\exp\left(-\frac{x^2}{2\sigma^2}\right)dx = 1 - \operatorname{erf}\left(\frac{b}{2^{3/2}\sigma}\right).$$

For the distribution to be normalized the above expression must equal one, which means that for every value of the impact parameter a new value for the normalization constant has to be calculated as follows

$$K_\cap = \frac{1}{1-\operatorname{erf}\left(\frac{b}{2^{3/2}\sigma}\right)}. \tag{3.9}$$

And thus we have our analytic representation for the normalized overlap

$$K_\cap(G_1 \cap G_2)(x,y) = \begin{cases} \frac{1}{1-\operatorname{erf}\left(\frac{b}{2^{3/2}\sigma}\right)}\frac{1}{2\pi\sigma^2}\exp\left(-\frac{(x-b)^2+y^2}{2\sigma^2}\right), & \text{if } x \le b/2 \\ \frac{1}{1-\operatorname{erf}\left(\frac{b}{2^{3/2}\sigma}\right)}\frac{1}{2\pi\sigma^2}\exp\left(-\frac{x^2+y^2}{2\sigma^2}\right), & \text{if } x > b/2 \end{cases} \tag{3.10}$$

The above description of the overlap model works fine if the sigmas of both Gaussians are the same, but as we later seek to impose radial fluctuations for the protons we need an expression that works even if the two Gaussians have different sigmas. Starting in a similar fashion we evaluate the plane of intersection between the Gaussians.

$$G_1(x,y) = G_2(x,y) \iff \frac{1}{2\pi\sigma_1^2}\exp\left(-\frac{x^2+y^2}{2\sigma_1^2}\right) = \frac{1}{2\pi\sigma_2^2}\exp\left(-\frac{(x-b)^2+y^2}{2\sigma_2^2}\right).$$

Rearranging this gives

$$\exp\left(\frac{(x-b)^2+y^2}{2\sigma_2^2}-\frac{x^2+y^2}{2\sigma_1^2}\right)=\left(\frac{\sigma_1}{\sigma_2}\right)^2.$$

Taking the natural logarithm of both sides gives

$$\frac{(x-b)^2+y^2}{2\sigma_2^2}-\frac{x^2+y^2}{2\sigma_1^2}=2\ln\left(\frac{\sigma_1}{\sigma_2}\right).$$

Which simplifies to

$$(\sigma_1^2-\sigma_2^2)(x^2+y^2)-2\sigma_1^2bx=4\sigma_1^2\sigma_2^2\ln\left(\frac{\sigma_1}{\sigma_2}\right)-\sigma_1^2b^2. \tag{3.11}$$

If $\sigma_1=\sigma_2$ this expression will reduce to $x=b/2$ as seen above. For the sake of brevity the following constants are defined

$$c_1\equiv\sigma_1^2-\sigma_2^2,\quad c_2\equiv-2\sigma_1^2b,\quad c_3\equiv4\sigma_1^2\sigma_2^2\ln\left(\frac{\sigma_1}{\sigma_2}\right)-\sigma_1^2b^2.$$

Which makes it clear that equation (3.11) is almost the equation for an ellipse.

$$c_1(x^2+y^2)+c_2x=c_3$$

Now that we have the equation for the plane of intersection we can define the more general (but not normalized) equations for the overlap model.

$$(G_1\cap G_2)(x,y)=\begin{cases}\frac{1}{2\pi\sigma_1^2}\exp\left(-\frac{x^2+y^2}{2\sigma_1^2}\right), & \text{if } c_1(x^2+y^2)+c_2x\le c_3\\ \frac{1}{2\pi\sigma_2^2}\exp\left(-\frac{(x-b)^2+y^2}{2\sigma_2^2}\right), & \text{if } c_1(x^2+y^2)+c_2x>c_3\end{cases} \tag{3.12}$$

3.2 Toy Model

The toy model simulates proton collision events with the Monte Carlo method and uses the hydrodynamical formula (2.5) and the geometry of the collision to calculate the elliptic flow.

Random positions are generated in each event from a probability density function in accordance with the three probability distributions as seen in equations (3.7), (3.8) and (3.10). It is worth mentioning that within the program the Gaussians are not infinitely decreasing but instead have a radial cut-off at 3σ. The randomly generated points are meant to simulate the transverse-space vertices for MPIs. The positions of these points can then be used to calculate the variance in each direction for each event. The curly brackets represents the average within an event

$$\sigma_x^2=\{x^2\}-\{x\}^2 \tag{3.13}$$

$$\sigma_y^2 = \{y^2\} - \{y\}^2$$
$$\sigma_{xy} = \{xy\} - \{x\}\{y\}.$$

This is used to calculate the area and participant eccentricity of the distribution for each event [14]

$$S = 4\pi\sqrt{\sigma_x^2\sigma_y^2 - \sigma_{xy}^2} \tag{3.14}$$

$$\epsilon_{part} \equiv \frac{\sqrt{(\sigma_y^2 - \sigma_x^2)^2 + 4\sigma_{xy}^2}}{\sigma_y^2 + \sigma_x^2}. \tag{3.15}$$

Which gives that the average eccentricity is

$$\epsilon_2\{2\} \equiv \sqrt{\langle\epsilon_{part}^2\rangle}. \tag{3.16}$$

The standard definition of the eccentricity of an ellipse is actually $\sqrt{1 - \sigma_x^2/\sigma_y^2}$. But this assumes that the semi-major axis is always perpendicular to the direction of the impact parameter. This is not the case as the eccentricity may be greater in other orientations.

The area is also averaged over the events and then the empirical formula from the RHIC (2.5) is used to calculate the elliptic flow of the final state hadrons.

The program starts by defining a plane of x- and y-values and then the probabilities associated with each position are generated according to the three models above. The code then defines 100 different values for the impact parameter ranging from 0 to 2.1 fm, for each of which 1000 events are generated and averaged over. Which means we generate 10^5 events for each model.

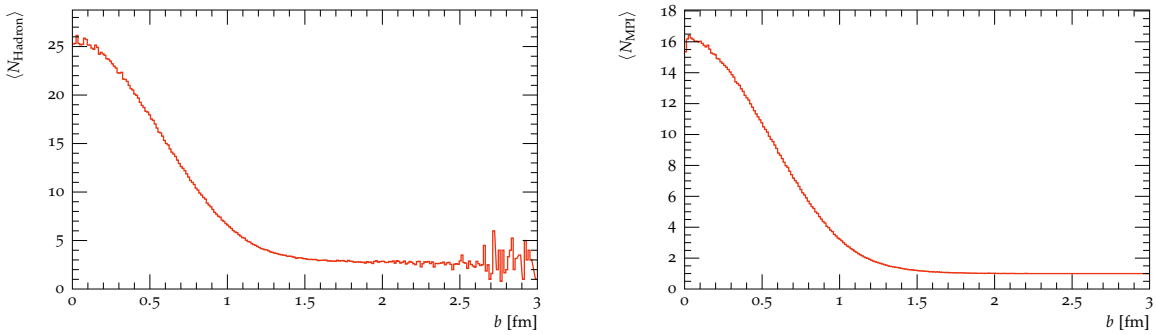

Figure 3: Some of the data in the toy model imported from PYTHIA. On the left we have the number of hadrons on the y-axis and impact parameter on the x-axis. On the right we have the number of MPIs on the y-axis and impact parameter on the x-axis.

The value for the total number of hadrons and charged particles for each value of the impact parameter is generated in and imported from PYTHIA with default settings and

a center of mass energy of 13 TeV. An option in the toy model consists of also importing the number of MPIs from PYTHIA, which means that the number of points generated will also vary with the impact parameter. Otherwise, they are kept constant at 10 MPI vertices each event regardless of impact parameter. In figure 3 are the plots of the data imported from PYTHIA, excluding the number of charged particles.

3.3 PYTHIA

The implementation of the overlap toy model into PYTHIA meant a few adaptations had to be made. Firstly, the randomly generated points should be defined from a continuous probability density function instead of a grid of points with associated probabilities like in the toy model. This was achieved by using the already defined Gaussian function in PYTHIA and using one for the x-axis and one for the y-axis. Then a flat random pointer picks a number between 0 and 1. If the number is less than 1/2 it generates the point from the first Gaussian, which means multiplying the point by the radius of the first proton. If the number is more than 1/2 it generates the point from the second Gaussian, which implies taking the product of the point and the second proton radius and adding on the impact parameter. This point selection for each Gaussian is also dependent on fulfilling the conditions of equation (3.11). Secondly, we want to impose radial fluctuations on the protons to study it's effects on anisotropic flow. This was achieved with using a third Gaussian random pointer with the mean of the radius of the proton and some standard deviation.

We will be comparing the default settings for generating MPI vertices in PYTHIA with and without shoving enabled. Then we will look at the effects of generating the MPI vertices from the overlap model with shoving enabled and compare this with the default settings. We will do this by making use of two RIVET analyses, which are means of validating Monte Carlo results by comparison to data. We will use one analysis for the CMS and one for ALICE [15, 1, 16].

4 Results

4.1 Toy Model

In figure 4 are the results from all three models and a constant number of MPIs plotted alongside data from 13 TeV collision experiments at CMS.

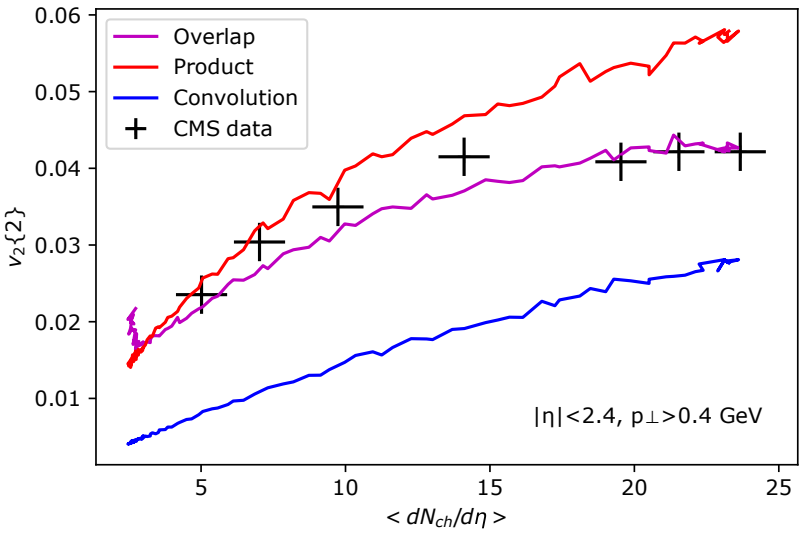

Figure 4: Results from the toy model without MPI dependence with elliptic flow on the y-axis and average number of charged particles on the x-axis.

In red we have the product model which seems to be predicting a higher eccentricity than the overlap and convolution model. In blue is the convolution model which notably predicts lower values than the other models. In purple is the overlap model which lies in between the product and convolution model. The common behaviour from all models are that the elliptic flow increases with the number of charged particles.

In figure 5 we have plots of the area and eccentricity of the spatial distributions as a function of impact parameter for all three models.

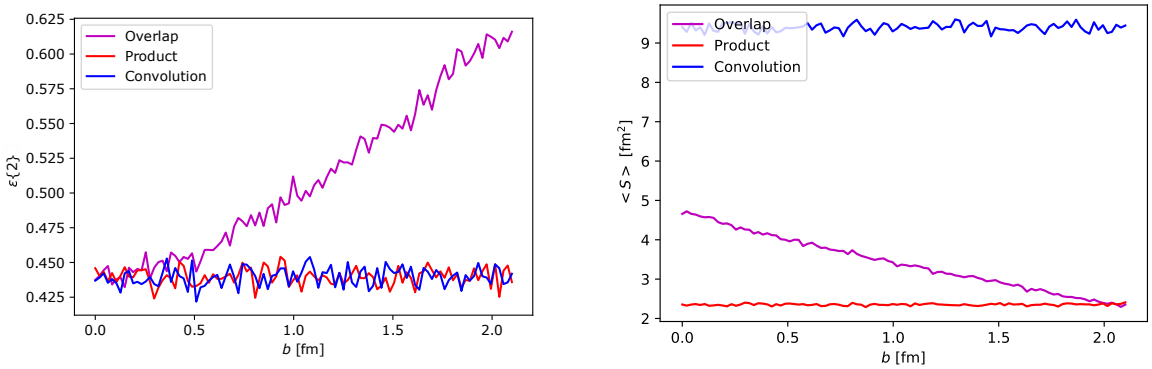

Figure 5: Two further results from the toy model without a dependence on the number of MPIs. On the left we have a plot of the eccentricity of the collision area on the y-axis and impact parameter on the x-axis. On the right we have a plot of the size of the collision area on the y-axis and impact parameter on the x-axis.

Here we can see that the product model produces a relatively low and, with exception to small fluctuation, constant value for the eccentricity and area of the arrangement. The convolution model also produces eccentricities and areas that are uncorrelated with impact parameter. It only differs from the product model in that it results in a significantly larger area with bigger fluctuations. Lastly, the overlap model starts out at around the same low eccentricity as the product and convolution model but increases with the impact parameter while its area decreases.

Below in figure 6 is the elliptic flow alongside number of charged particles again, this time with a dependence on the number of MPIs from PYTHIA enabled.

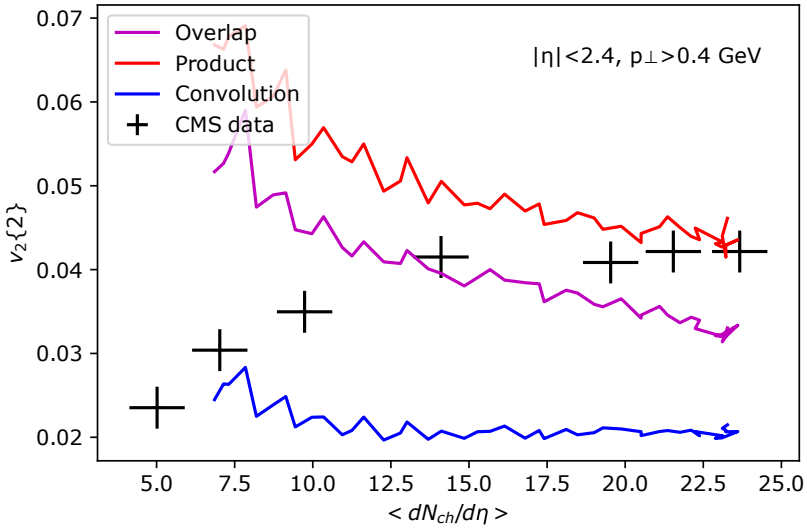

Figure 6: Results from the toy model with MPIs and elliptic flow as a function of average number of charged particles.

This time it looks very different. All three models have a decreasing elliptic flow as number of charged particles grows. Following, in figure 7, is the eccentricity and area as a function of impact parameter with MPI dependence enabled.

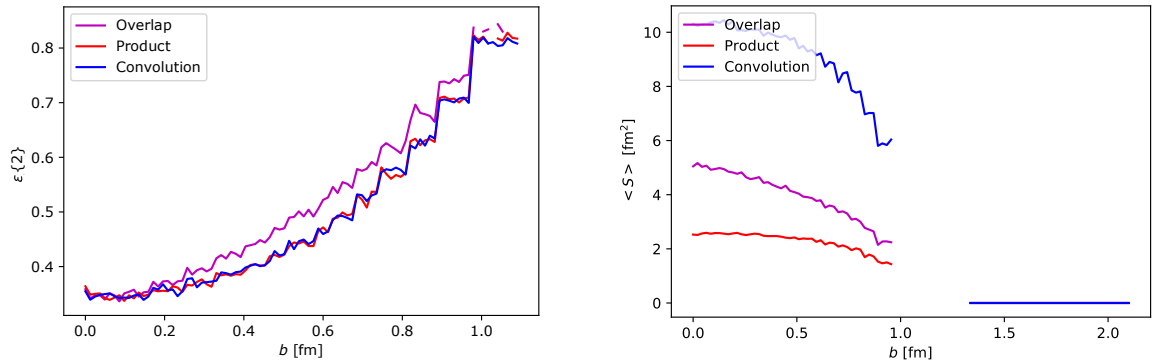

Figure 7: Two further results from the toy model with a dependence on the number of MPIs. On the left we have a plot of the eccentricity on the y-axis and impact parameter on the x-axis. On the right we have a plot of the area on the y-axis and impact parameter on the x-axis.

Now we see all models producing very similar results in terms of eccentricity. A curve increasing from a low eccentricity at $b = 0$ to having left the plot entirely already at around $b = 1.2$ fm. In the beginning the plot of the area has a resemblance to the one without MPIs enabled. The convolution model has the largest value followed by the overlap model and lastly the product model. Although, this time the area for all of the models is decreasing and around $b = 1$ they go to zero.

4.2 PYTHIA

In figure 8 are the results from the RIVET analyses in PYTHIA. On the left is the one for CMS with $V_{2\Delta} = v_2^2$ on the y-axis and number of charged particles on the x-axis. On the right is the one from ALICE with elliptic flow on the y-axis and number of charged particles on the x-axis. The overlap model is in red while the default convolution model is in blue.

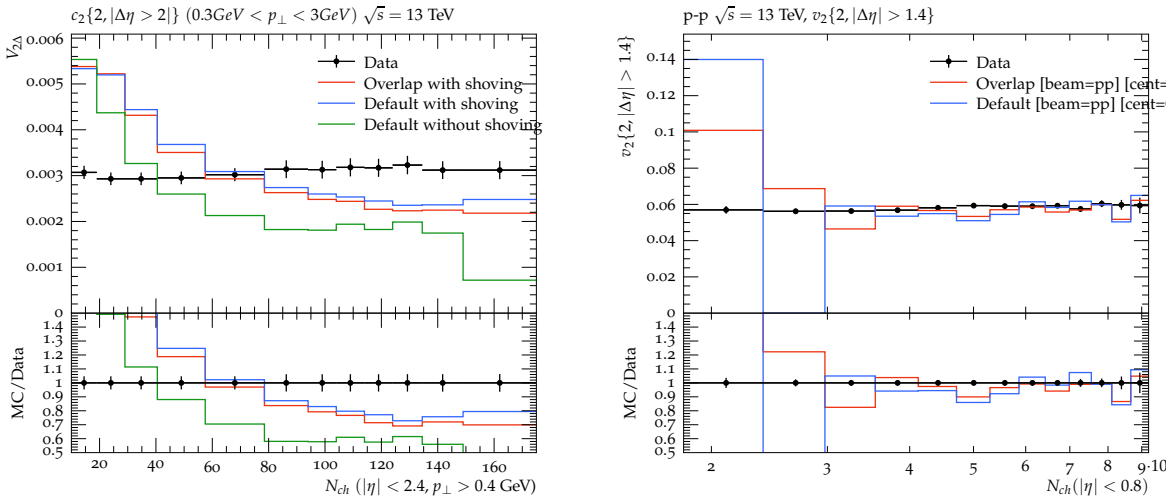

Figure 8: The results from PYTHIA. On the left we have the CMS analysis with number of charged particles on the x-axis and elliptic flow squared on the y-axis. On the right are the results from the ALICE analysis with number of charged particles on the x-axis and elliptic flow on y-axis.

As we can see in the CMS analysis the default without shoving is performing significantly worse than the convolution and overlap models with shoving. It seems that the overlap model is producing slightly lower values than the default, but they are largely quite similar. In the ALICE analysis the results for both models are even more similar and agree well with the data, except for at low number of charged particles where there are not enough statistics.

5 Conclusion

In summary, we have developed a model of the spatial probability density for parton vertices in the initial state of a pp-collision and used this to simulate elliptic flow. We have done this both in a hydrodynamical toy model based on QGP and in the PYTHIA event generator with string shoving. We then made use of data from the CMS and ALICE experiments to validate our results.

As can be see in figure 4 the overlap toy model performs very well in accordance with the data from CMS. From figure 5 it can be argued that this is because it is the only model that has intrinsic eccentricity as well as an area and eccentricity that depend on the impact parameter. More specifically we see the product and convolution producing fairly constant values for both the area and eccentricity while the overlap has an area that decreases and an eccentricity that increases as the impact parameter grows, which is closer to what we would expect from figure 1.

In figure 6 we see how importing data regarding MPIs from PYTHIA affects the results from the toy model. Making the number of MPIs dependent on the impact parameter is going to lead to the area decreasing and the eccentricity increasing for rising values of b. This means that the PYTHIA MPI model can simulate the effects of the impact parameter on the shape of the initial state, even when generating points from a symmetric distribution. But for higher values of the impact parameter the statistics used in equation (3.13) start to break down. When there is only one or two points the variance in each direction goes to zero. This causes the area to go to zero and the eccentricity to go to infinity for all models, as can be seen in figure 7. It therefore does not make much sense to speak of collective mechanisms at a low number of particles.

The reason all the models produce such similar eccentricities is because the difference between the models at a constant number of MPIs is much smaller than the effects of decreasing the number of MPIs. But even though all of the models produce very similar results in terms of eccentricity, the difference in area is still tangible, this is due to the convolution model drawing samples from a Gaussian with twice the variance of the protons and four times the variance of the product model. In fact, since all models use the same data for the number of charged particles, hadrons and MPIs as well as produce very similar results in terms of eccentricity this difference in area is most significantly contributing to the difference in elliptic flow between the models.

On the left in figure 8 we see the results from the CMS analysis using the PYTHIA implementation of the overlap model with string shoving and the convolution model with and without string shoving as well as the CMS data. The string shoving makes a clear improvement as compared with the data. It is possible that the slight difference we observe between the default convolution and the overlap model with shoving could be caused by their difference in area and eccentricity. On the right in figure 8 we see the results from the ALICE analysis, here the difference is too small to make any declarative statement about which model performed better. The reason for the CMS analysis demonstrating a

more clear difference between the models is most likely due to that squaring the amount of elliptic flow is going to enlarge any differences between the models. The CMS analysis also takes a broader range of rapidities into account which is going to highlight eventual differences through the larger sample size. Although, since the ALICE analysis deals with a lower number of charged particles we might have expected to see a greater difference there since as the number of charged particles decreases the difference between the overlap and convolution becomes more substantial, but this does not seem to meaningfully represent itself in the results.

These results are gotten from high statistic runs with close to a billion events so they ought to be representative of each model. The reason the toy model shows a much greater difference between the convolution and overlap is probably because it includes a lot of generalizations surrounding the non-flow contributions in scattering and hadronization processes that might even out some of the differences. PYTHIA models a wide array of hard and soft processes and it seems that these are more heavily contributing to the results in elliptic flow than the difference between the convolution and overlap geometries.

In the interest of future research it may be worthwhile to study the effects of the overlap model on the third flow harmonic, triangular flow, which is mainly caused by radial fluctuations in the protons. Since the overlap model has a unique way of modelling fluctuations in the collision region one might observe a more significant difference from the default settings in measurements of v_3. As an extension of this, one might look into the effects of the overlap model on the correlations between elliptic and triangular flow, their symmetric cumulants, which carries information about how the system reacts to both the initial spatial configuration of the protons and their fluctuations. One could also try estimating the parameters of the model, like the proton radius, by examining measurements of cross sections.

This thesis has shown a large effect on the initial state geometry of pp-collisions by using the overlap region of two Gaussians to generate spatial vertices for MPIs, as can be seen in figure 5. Ultimately the effects of this on simulating elliptic flow with string shoving was negligible. But because the geometric differences between the overlap and convolution are so substantial there likely is a final state observable where this is noticeable. One place to start is by analysing other flow harmonics and symmetric cumulants with the overlap model. Research could also be extended by continuing to run simulations of elliptic flow and creating more new anisotropic geometries to sample MPI vertices from. Although this may be a dead end because of the lack of significant differences in elliptic flow between the convolution model and overlap model, which already differ greatly in terms of area and eccentricity.

References

[1] Vardan Khachatryan et al. Evidence for collectivity in pp collisions at the LHC. *Phys. Lett. B*, 765:193–220, 2017.

[2] Rajeev S. Bhalerao and Jean-Yves Ollitrault. Eccentricity fluctuations and elliptic flow at RHIC. *Phys. Lett. B*, 641:260–264, 2006.

[3] K. H. Ackermann et al. Elliptic flow in Au + Au collisions at (S(NN))**(1/2) = 130 GeV. *Phys. Rev. Lett.*, 86:402–407, 2001.

[4] R. Derradi de Souza, Tomoi Koide, and Takeshi Kodama. Hydrodynamic Approaches in Relativistic Heavy Ion Reactions. *Prog. Part. Nucl. Phys.*, 86:35–85, 2016.

[5] Christian Bierlich, Smita Chakraborty, Gösta Gustafson, and Leif Lönnblad. Setting the string shoving picture in a new frame. *JHEP*, 03:270, 2021.

[6] Torbjörn Sjöstrand. The Development of MPI Modeling in Pythia. *Adv. Ser. Direct. High Energy Phys.*, 29:191–225, 2018.

[7] Torbjörn Sjöstrand, Stefan Ask, Jesper R. Christiansen, Richard Corke, Nishita Desai, Philip Ilten, Stephen Mrenna, Stefan Prestel, Christine O. Rasmussen, and Peter Z. Skands. An introduction to PYTHIA 8.2. *Comput. Phys. Commun.*, 191:159–177, 2015.

[8] Ingo Sick. Proton charge radius from electron scattering. *Atoms*, 6(1):2, 2018.

[9] S. Sapeta and Krzysztof J. Golec-Biernat. Total, elastic and diffractive cross sections at LHC in the Miettinen-Pumplin model. *Phys. Lett. B*, 613:154–161, 2005.

[10] Michael L. Miller, Klaus Reygers, Stephen J. Sanders, and Peter Steinberg. Glauber modeling in high energy nuclear collisions. *Ann. Rev. Nucl. Part. Sci.*, 57:205–243, 2007.

[11] A. Bialas. Wounded nucleons, wounded quarks: An update. *J. Phys. G*, 35:044053, 2008.

[12] Hans-Joachim Drescher, Adrian Dumitru, Clement Gombeaud, and Jean-Yves Ollitrault. The Centrality dependence of elliptic flow, the hydrodynamic limit, and the viscosity of hot QCD. *Phys. Rev. C*, 76:024905, 2007.

[13] Christian Bierlich, Gösta Gustafson, and Leif Lönnblad. Collectivity without plasma in hadronic collisions. *Phys. Lett. B*, 779:58–63, 2018.

[14] Emil Avsar, Christoffer Flensburg, Yoshitaka Hatta, Jean-Yves Ollitrault, and Takahiro Ueda. Eccentricity and elliptic flow in proton–proton collisions from parton evolution. *Phys. Lett. B*, 702:394–397, 2011.

[15] Christian Bierlich et al. Robust Independent Validation of Experiment and Theory: Rivet version 3. *SciPost Phys.*, 8:026, 2020.

[16] Shreyasi Acharya et al. Investigations of Anisotropic Flow Using Multiparticle Azimuthal Correlations in pp, p-Pb, Xe-Xe, and Pb-Pb Collisions at the LHC. *Phys. Rev. Lett.*, 123(14):142301, 2019.